Numerical study of the Boussinesq approach validity for natural convection and surface thermal radiation in an open cavity

M. Montiel Gonzalez[a], J. Hinojosa Palafox[b], and C. Estrada Gasca[a]
[a]*Institute of Renewable Energies, Universidad Nacional Autónoma de México, Apartado Postal 34, Temixco, 62580, Morelos, Mexico, Tel. +52 (55) 56229744 e-mail: cestrada@cie.unam.mx*
[b]*Departament of Chemical Engineering and Metallurgy, University of Sonora, Blvd. Luis Encinas y Rosales s/n, Hermosillo, 83000, Sonora, México, Tel. +52 (662) 2592106 e-mail: fhinojosa@iq.uson.mx*

Received 22 February 2013; accepted 30 August 2013

In this work the validity of the Boussinesq approach for the heat transfer calculations in an open cavity considering natural convection and surface thermal radiation is studied. Numerical calculations were conducted for Rayleigh number (Ra) values in the range of 10^4 -10^6. The temperature difference between the hot wall and the bulk fluid (ΔT) was varied between 10 and 100 K, and was represented as a dimensionless temperature difference (φ). The deviations for the temperature fields and fluid flow patterns, between variable properties and Boussinesq approach are noticeable for φ=0.333. For total Nusselt numbers, the results with Boussinesq approach and variable properties, indicates deviations within 0.22 % (Ra=10^5 and φ=0.033) and 5 % (Ra=10^4 and φ=0.333).

Keywords: Boussinesq approach; natural convection; thermal radiation; open cavity.

PACS: 44.25.+f, 44.40.+a

1. Introduction

Heat transfer in open cavities is relevant in several thermal engineering applications. Some examples include the cooling of electronic devices and the design of solar concentrators receivers, among others. In the literature, over the last forty years, a large number of numerical studies have been reported to describe the heat transfer in open cavities [1-35]. These studies can be categorized as: (a) natural convection in an open cavity with isothermal walls [1-6], (b) natural convection in an open cavities with adiabatic walls and isothermal at the wall facing the aperture [7-16], (c) combined natural convection with conduction or surface thermal radiation in two-dimensional open cavities [17-27], (d) natural convection in partially open cavities [28-30] and (e) natural convection in a cavity with two open sides (using a symmetry plane) [31-36]. The investigations of the heat transfer by combined natural convection and surface thermal radiation are briefly presented next.

Lage *et al*. [17] studied numerically the heat transfer by natural convection and surface thermal radiation in a two-dimensional open top cavity; the authors solved separately the steady state equations of natural convection and thermal radiation, assuming a temperature distribution on the vertical adiabatic wall. Balaji and Venkateshan [18] obtained steady state numerical results for the interaction of surface thermal radiation with free convection in an open top cavity, whose left wall was considered isothermal, and the right and bottom walls were adiabatic and their temperature distributions were determined by an energy balance between convection and radiation in each surface element of the walls. Surface radiation was found to alter the basic flow pattern as well as the overall thermal performance substantially. Balaji and Venkateshan [19] developed a numerical study of combined conduction, natural convection and surface thermal radiation in an open top cavity. Radiation was found to enhance overall heat transfer substantially (50–80 %) depending on the radiative parameters.

Singh and Venkateshan [20] presented a numerical study of steady combined laminar natural convection and surface radiation in a two-dimensional side-vented open cavity. The numerical investigation provides evidence of the existence of thermal boundary layers along adiabatic walls of the cavity as a consequence of the interaction of natural convection and surface radiation. Hinojosa *et al*. [21] reported numeric results of Nusselt numbers for a tilted open square cavity, considering natural convection and surface thermal radiation. The results were obtained for a Rayleigh range from 10^4 to 10^7 and for an inclination angles range of the cavity from 0 to 180°. The results show that convective Nusselt number changes substantially with the inclination angle of the cavity, while the radiative Nusselt number is insensitive to the orientation change of the cavity.

Hinojosa *et al*. [22] presented numeric results for transient and steady-state natural convection and surface thermal radiation in a horizontal open square cavity. The results were obtained for a Rayleigh range from 10^4 to 10^7. The results show that the radiative exchange between the walls and the aperture increases considerably the total average Nusselt number, from around 94% to 125%. Nouanegue *et al*.

[23] investigated conjugate heat transfer by natural convection, conduction and radiation in open cavities in which a uniform heat flux is applied to the inside surface of the solid wall facing the opening. The influence of the surface radiation is to decrease the heat fluxes by natural convection and conduction while the heat flux by radiation increases with increasing surface emissivity.

Hinojosa [24] reported the numerical calculations of heat transfer by natural convection and surface radiation in a tilted open shallow cavity. The results in the steady state were obtained for a Rayleigh number range from 10^5 to 10^7, inclination angles from 45 to 135° and aspect ratios equal to 2 and 4. It was found that the exchange of thermal radiation between walls is considerably more relevant that the convective phenomenon for an inclination angle of 135°. Oscillations in the convective Nusselt number were observed for inclination angles of 45° (AR=4) and 90° (AR of 2 and 4). Wang *et al*. [25] studied the combined heat transfer by natural convection, conduction, and surface radiation in an open cavity. The unsteady-state flow and heat transfer exhibited periodic oscillating or chaotic behaviors due to formation of the thermal plumes at the bottom wall. If the formation of thermal plumes is periodic, the oscillations of flow and heat transfer are also periodic.

However because rigorous mathematical models aimed at describing natural convection and surface thermal radiation are complex, the previously described studies have used the Boussinesq approximation to predict the fluid motion and heat transfer behavior inside the open cavity. This approximation is commonly understood to consist of the following [37]: (a) density is assumed constant except in the buoyancy term in the momentum equations where it is varied linearly, (b) All other fluid properties in the governing equations are assumed to be constant, (c) Viscous dissipation is assumed negligible. Nevertheless the accuracy of the Boussinesq approximation has not been established to study the natural convection coupled with surface thermal radiation in an open cavity.

Considering the above, this work is focused to analyze the validity of the Boussinesq approach to study the heat transfer by natural convection and surface thermal radiation in a square open cavity. The governing equations were solved with variable properties and Boussinesq approach, for Rayleigh number (Ra) values in the range of 10^4-10^6. The temperature difference between the hot wall and the bulk fluid (ΔT) was varied between 10 and 100 K and it was represented as a dimensionless temperature difference (φ). The obtained results of the fluid motion pattern, temperature fields and heat transfer were compared and discussed.

2. Model formulation and numerical solution

In this work, the natural convection and surface thermal radiation in a two-dimensional, square open cavity of length L is considered. The system is schematically shown in Fig. 1. The cavity has two horizontal adiabatic walls. The vertical wall is kept at constant temperature T_H, while the surrounding fluid interacting with the aperture is at a fixed ambient temperature (T_∞) of 300 K which was lower than T_H. The fluid was radiatively non-participating and the walls of the cavity were considered as black bodies. The ambient fluid is air at atmospheric pressure and was assumed Newtonian and an ideal gas. The fluid flow is assumed to be laminar and at steady state.

From the above considerations, the governing equations describing the fluid motion inside the cavity under steady state conditions may be written as follows [38]:
continuity:

$$\frac{\partial}{\partial x}(\rho u)+\frac{\partial}{\partial y}(\rho v)=0 \tag{1}$$

$x-$Momentum:

$$\frac{\partial(\rho uu)}{\partial x}+\frac{\partial(\rho uv)}{\partial y}=-\frac{\partial p}{\partial x}+\frac{\partial}{\partial x}\Big[2\mu\frac{\partial u}{\partial x} -\frac{2}{3}\mu\left(\frac{\partial u}{\partial x}+\frac{\partial v}{\partial y}\right)\Big]+\frac{\partial}{\partial y}\left[\mu\left(\frac{\partial u}{\partial y}+\frac{\partial v}{\partial x}\right)\right] \tag{2}$$

$y-$Momentum:

$$\frac{\partial(\rho vu)}{\partial x}+\frac{\partial(\rho vv)}{\partial y}=-\frac{\partial p}{\partial y}+\frac{\partial}{\partial y}\Big[2\mu\frac{\partial v}{\partial y} -\frac{2}{3}\mu\left(\frac{\partial u}{\partial x}+\frac{\partial v}{\partial y}\right)\Big]+\frac{\partial}{\partial x}\left[\mu\left(\frac{\partial u}{\partial y}+\frac{\partial v}{\partial x}\right)\right]+\rho g \tag{3}$$

Energy:

$$\frac{\partial(uCpT)}{\partial x}+\frac{\partial(vCpT)}{\partial y}=\frac{\partial}{\partial x}\left(k\frac{\partial T}{\partial x}\right)+\frac{\partial}{\partial y}\left(k\frac{\partial T}{\partial y}\right) \tag{4}$$

The application of the Boussinesq approximation simplifies the equations (1-4) as follows:

$$\frac{\partial u}{\partial x}+\frac{\partial \mathrm{v}}{\partial y}=0 \tag{5}$$

$$\frac{\partial(uu)}{\partial x}+\frac{\partial(u\mathrm{v})}{\partial y}=-\frac{1}{\rho}\frac{\partial p}{\partial x}+\nu\left(\frac{\partial^2 u}{\partial x^2}+\frac{\partial^2 u}{\partial y^2}\right) \tag{6}$$

$$\frac{\partial(u\mathrm{v})}{\partial x}+\frac{\partial(\mathrm{vv})}{\partial y}=-\frac{1}{\rho}\frac{\partial p}{\partial x} +\nu\left(\frac{\partial^2 \mathrm{v}}{\partial x^2}+\frac{\partial^2 \mathrm{v}}{\partial y^2}\right)+\beta g(T-T_\infty) \tag{7}$$

$$\frac{\partial(uT)}{\partial x}+\frac{\partial(\mathrm{v}T)}{\partial y}=\alpha\left(\frac{\partial^2 T}{\partial x^2}+\frac{\partial^2 T}{\partial y^2}\right) \tag{8}$$

where ρ, μ, ν, α, β and k are: the density, the dynamic viscosity, the thermal diffusivity, the kinematic viscosity, the thermal expansion coefficient and the thermal conductivity respectively; whereas g is the acceleration of gravity.

The hydrodynamic boundary conditions used in this work are:

$$u(0, 0 \le y \le L) = u(0 \le x \le L, 0) = u(0 \le x \le L, L) = 0 \quad (9)$$

$$v(0, 0 \le y \le L) = v(0 \le x \le L, 0) = v(0 \le x \le L, L) = 0 \quad (10)$$

$$\left(\frac{\partial u}{\partial x}\right)_{x=L} = \left(\frac{\partial v}{\partial x}\right)_{x=L} = 0 \quad (11)$$

Equations (9) and (10) assume non-slip conditions at the solid walls, whereas Eq. (11) assume that in the aperture plane no velocity gradients and thus no momentum transfer occurs at this location [10].

The thermal boundary conditions were set as follows:

$$T(0, 0 \le y \le L) = T_H \quad (12)$$

$$-k\left(\frac{\partial T}{\partial y}\right)_{0<\mathrm{x}\le \mathrm{L}, \mathrm{y}=0} = q_r(0 < \mathrm{x} \le \mathrm{L}, 0) \quad (13)$$

$$-k\left(\frac{\partial T}{\partial y}\right)_{0<\mathrm{x}\le \mathrm{L}, \mathrm{y}=\mathrm{L}} = q_r(0 < \mathrm{x} \le \mathrm{L}, \mathrm{L}) \quad (14)$$

$$T(L, 0 < y < L) = 0 \quad \text{if} \quad u < 0 \quad \text{or} \quad \left(\frac{\partial T}{\partial x}\right)_{\mathrm{x}=\mathrm{L}, 0<y<\mathrm{L}} = 0 \quad \text{if} \quad u > 0 \quad (15)$$

Equation (12) establishes that the vertical wall of the cavity is at constant temperatures T_H, whereas Eqs. (13) and (14) were obtained applying an energy balance on the adiabatic surfaces by considering the transmission of heat by radiation and convection [22]. Finally Equation (15) considers that the incoming fluid enters to the cavity at ambient temperature, while for the fluid leaving the cavity the thermal conduction is negligible [8].

To obtain the net radiative heat fluxes over the walls, the walls were divided in elements according to the mesh used to solve Eqs. (13)-(14) and the radiosity-irradiance formulation was applied. The general radiosity equation for the i^{th} element of the cavity may be written as

$$J_i = \varepsilon_i \sigma T_i^4 + (1 - \varepsilon_i) \sum_{j=1}^{N} F_{ij} J_j \quad (16)$$

where, ε_i is the emissivity of the surface element; F_{ij} is the view factor from the i^{th} element to the j^{th} element of the cavity, while N is the total number of elements along the cavity. View factors were evaluated using Hottel's crossed string method [39]. The net radiative flux (q_r) for the i^{th} element of any of the walls of the cavity was calculated by

$$q_{ri} = J_i - q_{Ii} \quad (17)$$

where q_{ri} is the net radiative heat flux, J_i is the radiosity of the corresponding element and q_{Ii} is the irradiance energy that arrives to the i^{th} element coming from the rest of the elements of the cavity.

The fluid properties were obtained at the mean temperature of the isothermal wall and the ambient temperature when Boussinesq approach is considered; whereas for variable properties, the dependency of the fluid properties with temperature was considered as follows.

The air density (ρ) was obtained from the ideal-gas equation:

$$\rho(p, T) = \frac{p}{R \cdot T} \quad (18)$$

The dynamic viscosity of air was computed from the Sutherland equation and the thermal conductivity of air k with an empirical relationship [38]:

$$\mu(T) = \frac{14.58 \times 10^{-7} T^{3/2}}{110.4 + T} \quad (19)$$

$$k(T) = \frac{2.6482 \times 10^{-3} T^{1/2}}{1 + 245.4 \times 10^{-(12/T)}/T} \quad (20)$$

For the specific heat capacity (C_p) the following equation was obtained from experimental data [40]:

$$Cp(T) = 955.1141 + 6.7898 \times 10^{-2} T + 1.6576 \times 10^{-4} T^2 - 6.7863 \times 10^{-8} T^3 \quad (21)$$

in above fluid properties equations p is the fluid pressure in Pa, T is the absolute temperature in K, R is the ideal gas constant for air equal to 287 J/kg·K, μ is viscosity in Pa·s, k is in W/m·K and C_p in J/kg·K.

To generalize the validity of the numerical results, the following dimensionless variables were defined:

$$X = \frac{x}{L} \quad Y = \frac{y}{L} \quad U = \frac{u}{U_0} \quad V = \frac{v}{U_0} \quad (22)$$

$$\theta = \frac{T - T_\infty}{T_H - T_\infty} \qquad \varphi = \frac{T_H - T_\infty}{T_\infty}$$

$$\mathrm{Pr} = \frac{\nu}{\alpha} \qquad Ra = \mathrm{Pr}\,\frac{g\beta(T_H - T_\infty)L^3}{\nu^2}$$

where X and Y are the dimensionless horizontal and vertical length of the cavity, respectively, U and V are the dimensionless horizontal and vertical components of the velocity vector, θ is the dimensionless fluid temperature, ϕ is the dimensionless temperature difference between the hot wall and the ambient air, Pr is the Prandtl number and Ra is the Rayleigh number. The ϕ parameter is related with the non-buoyancy influence of the temperature field on the flow field, whereas the reference velocity U_o is connected with the buoyancy force and was defined as $U_0 = (g\beta L(TH - T\infty))^{1/2}$. It is noted that the fluid properties included in the definitions of U_0 and both Ra and Pr numbers were computed at the mean temperature of the isothermal wall and the ambient temperature.

The convective Nusselt number is defined as the ratio between the heat flux at the hot wall in the presence of natural convection and the heat flux due to conduction only, *i.e.*,

$$Nu_c = \frac{q_{\text{convection}}}{q_{\text{conduction}}} = \frac{-k_{\text{wall}} \left(\frac{\partial T}{\partial x}\right)_{x=0,0\leq y\leq L}}{k_{\text{average}} \left(T_H - T_\infty\right)/L} \tag{23}$$

where k_{wall} was obtained at T_H, and $k_{average}$ was computed at the average temperature between the isothermal wall and the ambient air.

The average convective Nusselt number in the cavity was calculated by integrating the local Nusselt number over the length of the isothermal wall:

$$\overline{Nu_c} = \int_0^1 Nu_c \, dY \tag{24}$$

The radiative Nusselt number is defined as the ratio between the radiative heat flux at the hot wall and the heat flux due to conduction only, then:

$$Nu_r = \frac{q_{\text{radiation}}}{q_{\text{conduction}}} = \frac{q_r(0, 0 < y \leq L)}{k_{\text{average}} \left(T_H - T_\infty\right)/L} \tag{25}$$

The average radiative Nusselt number was obtained integrating the radiative Nusselt numbers over the isothermal wall, by the following mathematical relationship

$$\overline{Nu_r} = \int_0^1 Nu_r \, dY \tag{26}$$

The total average Nusselt number ($\overline{Nu_t}$) was calculated by summing the average convective Nusselt number and the average radiative Nusselt number.

3. Numerical procedure

The Eqs. (1)-(8) were numerically solved by means of the finite-volume method [38]. The equations were discretized

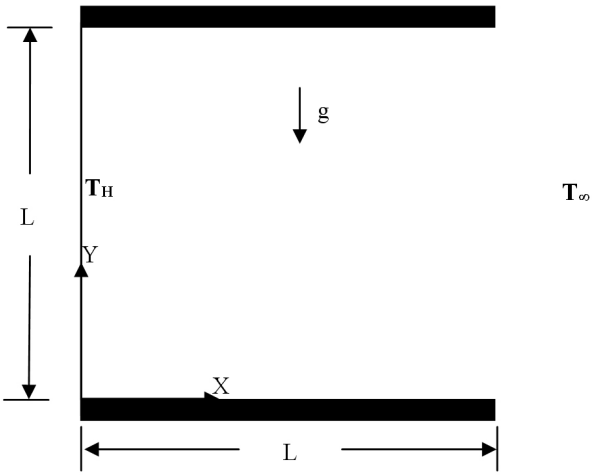

FIGURE 1. Scheme of the physical model.

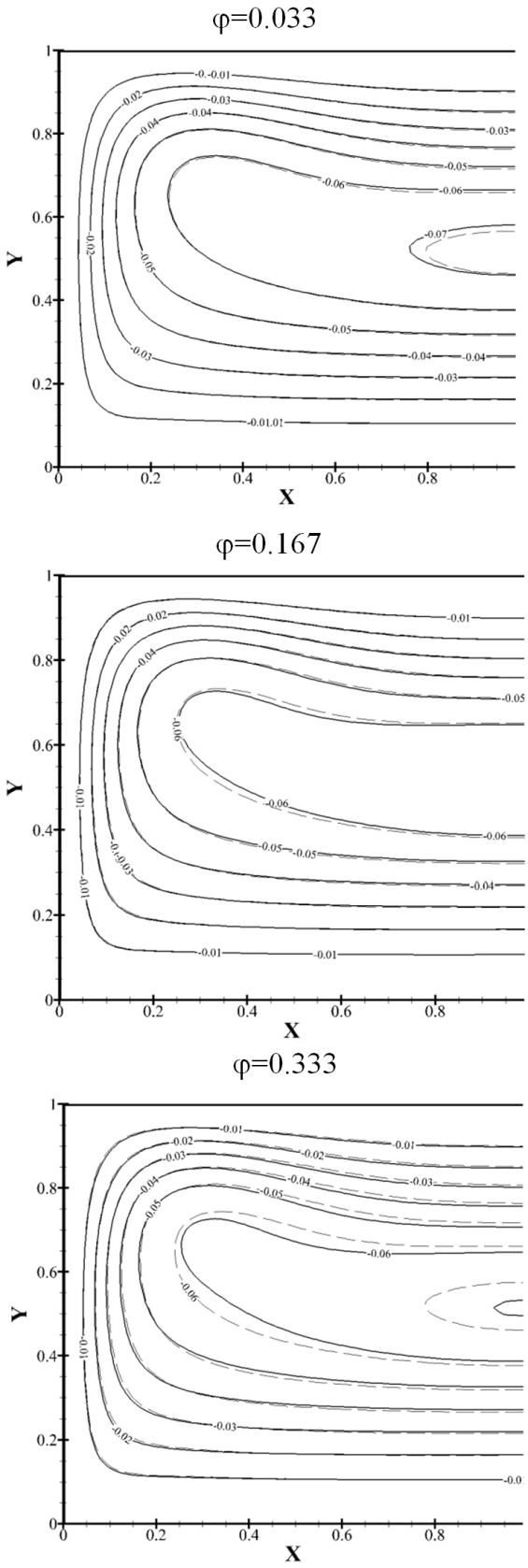

FIGURE 2. Streamlines contours for Ra=10^5. The continuous line corresponds to variable properties and the dotted line to the Boussinesq approach.

TABLE I. Mesh independence study in the open cavity.

Mesh size	**Nu**$_C$	**Nu**$_r$	**Nu**$_T$	**Difference** (%) **for Nu**$_C$	**Difference** (%) **for Nu**$_r$	**Difference** (%) **for Nu**$_T$
40×40	13.29	13.94	27.23			
5050	12.93	13.53	26.46	2.71	2.94	2.83
6060	12.72	13.15	25.87	1.62	2.81	2.23
70×70	12.66	13.07	25.73	0.47	0.61	0.54

TABLE II. Comparison of average Nusselt numbers reported in the literature for ϕ=0.033.

	This work (variable properties)			**Hinojosa *et al* [25] (Boussinesq)**		
Ra	$\overline{Nu_c}$	$\overline{Nu_r}$	$\overline{Nu_t}$	$\overline{Nu_c}$	$\overline{Nu_r}$	$\overline{Nu_t}$
10^4	3.05	3.54	6.39	2.98	3.72	6.70
10^5	6.36	7.64	13.70	6.40	8.02	14.42
10^6	12.32	16.42	28.14	12.43	17.29	29.72

into a large number of uniform control volumes using a staggered mesh. The position of the grid nodes was calculated using a stretching function, in orderto place nodes near the isothermal wall. The interpolation of the convective terms was performed with the power-law scheme [41], whereas the diffusive terms were interpolated with a centered-difference scheme. The SIMPLEC algorithm [42] was used to couple the continuity and momentum equations. The resulting system of linear algebraic equations was solved with the modified strongly implicit procedure (MSIP) [43].

The grid independence study was conducted by setting Ra=106 and φ=0.333. Table I shows the corresponding average values of the Nusselt numbers obtained for the numerical grids tested. In this study, independence of the numerical results from the grid size was assumed when the difference in the Nusselt numbers computed between two consecutive grids was less than 1%. Based on the values reported in Table I, a non-uniform grid of 70×70 nodes was selected

The verification of the present code was accomplished by comparing the model predictions with previous calculations reported in the literature [22]. Table II shows the comparison of the Nusselt numbers, where the governing equations were solved considering temperature-dependent fluid properties and setting ΔT=10 K. It is observed that the absolute percentage difference for average convective Nusselt number was between 0.6 % (Ra=10^5) and 2.3% (Ra=10^4), whereas for average radiative Nusselt number was between 4.8 % (Ra=10^4) and 5.0 % (Ra=10^6). Based on above results the present numerical code was considered as verified.

4. Discussion of results

For the purpose of the present analysis, the Rayleigh number (Ra) was varied in the range of 10^4 to 10^6, and the dimensionless temperature difference φ was varied in the range of 0.033 to 0.333. The latter corresponds to dimensional temperature difference ΔT in the range of 10-100 K.

Figure 2 presents the computed flow patterns in the open cavity and streamlines contours as function of φ for Ra=10^5. Every graph reports the corresponding results with variable properties (continuous line) and with the Boussinesq assumption (dotted line). In general the fluid enters from the bottom of the aperture, circulates clockwise direction following the shape of the cavity driven by the buoyant force acting upon the fluid, and leaves by the upper of the aperture. It can be observed for φ=0.033 and φ=0.167, a good agreement between the streamlines contours with variable properties and Boussinesq approximation. However the further increment to φ=0.333 produces an appreciable deviation between both results, in the streamlines located at the center of the cavity.

The influence of the Rayleigh number on the fluid flow pattern is shown in Figure 3, for φ=0.033 and φ=0.333. The streamline patterns are very similar for the three Rayleigh

TABLE III. Average Nusselt numbers on the hot wall of the open cavity computed with variable properties.

	Ra=10^4			**Ra=10^5**			**Ra=10^6**		
ϕ	$\overline{Nu_c}$	$\overline{Nu_r}$	$\overline{Nu_t}$	$\overline{Nu_c}$	$\overline{Nu_r}$	$\overline{Nu_t}$	$\overline{Nu_c}$	$\overline{Nu_r}$	$\overline{Nu_t}$
0.033	3.05	3.54	6.39	6.36	7.64	13.7	12.32	16.42	28.1
0.167	3.12	2.58	5.70	6.49	5.70	12.1	12.56	12.17	24.7
0.333	3.19	2.82	6.01	6.81	6.20	13.0	12.66	13.07	25.7

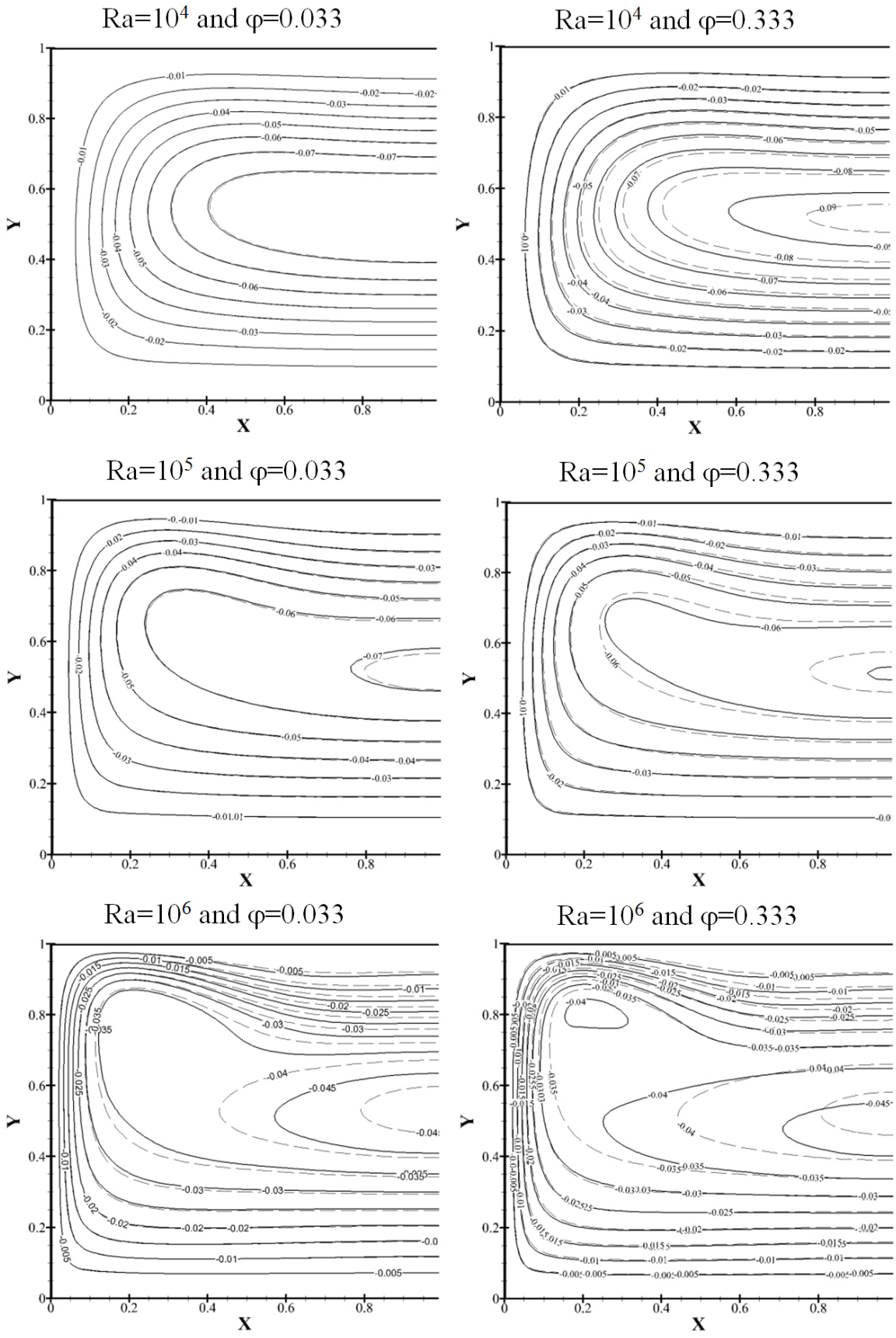

FIGURE 3. Streamlines contours for the different Rayleigh numbers. The continuous line corresponds to variable properties and the dotted line to the Boussinesq approach.

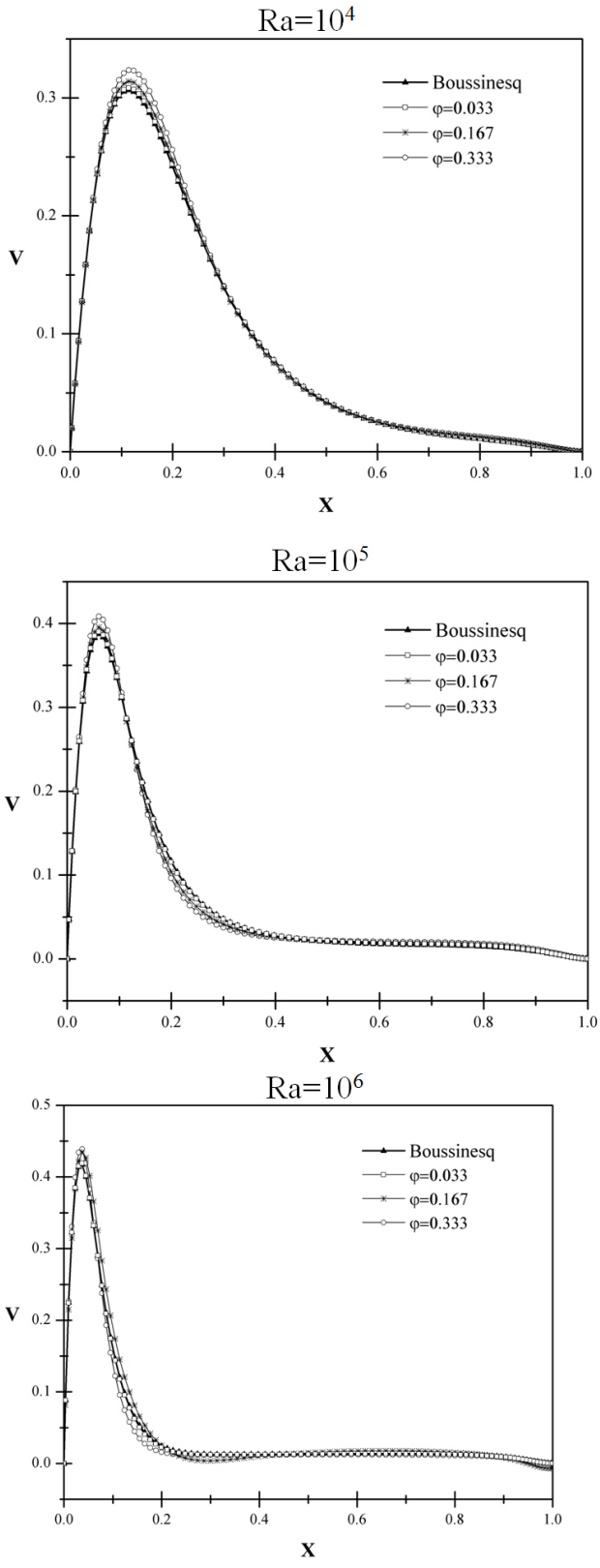

FIGURE 4. Profiles of the dimensionless vertical component of velocity at Y=0.5.

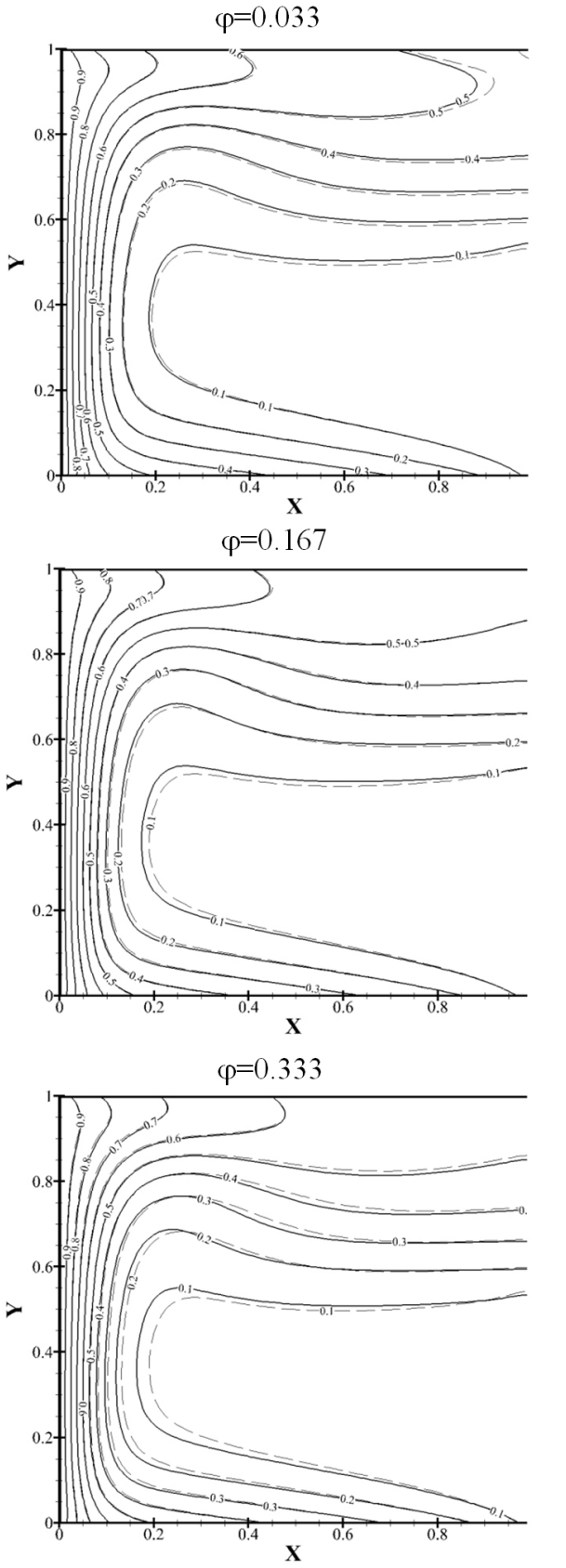

FIGURE 5. Isoterm contours for Ra=10^5. The continuous line corresponds to variable properties and the dotted line to the Boussinesq approach.

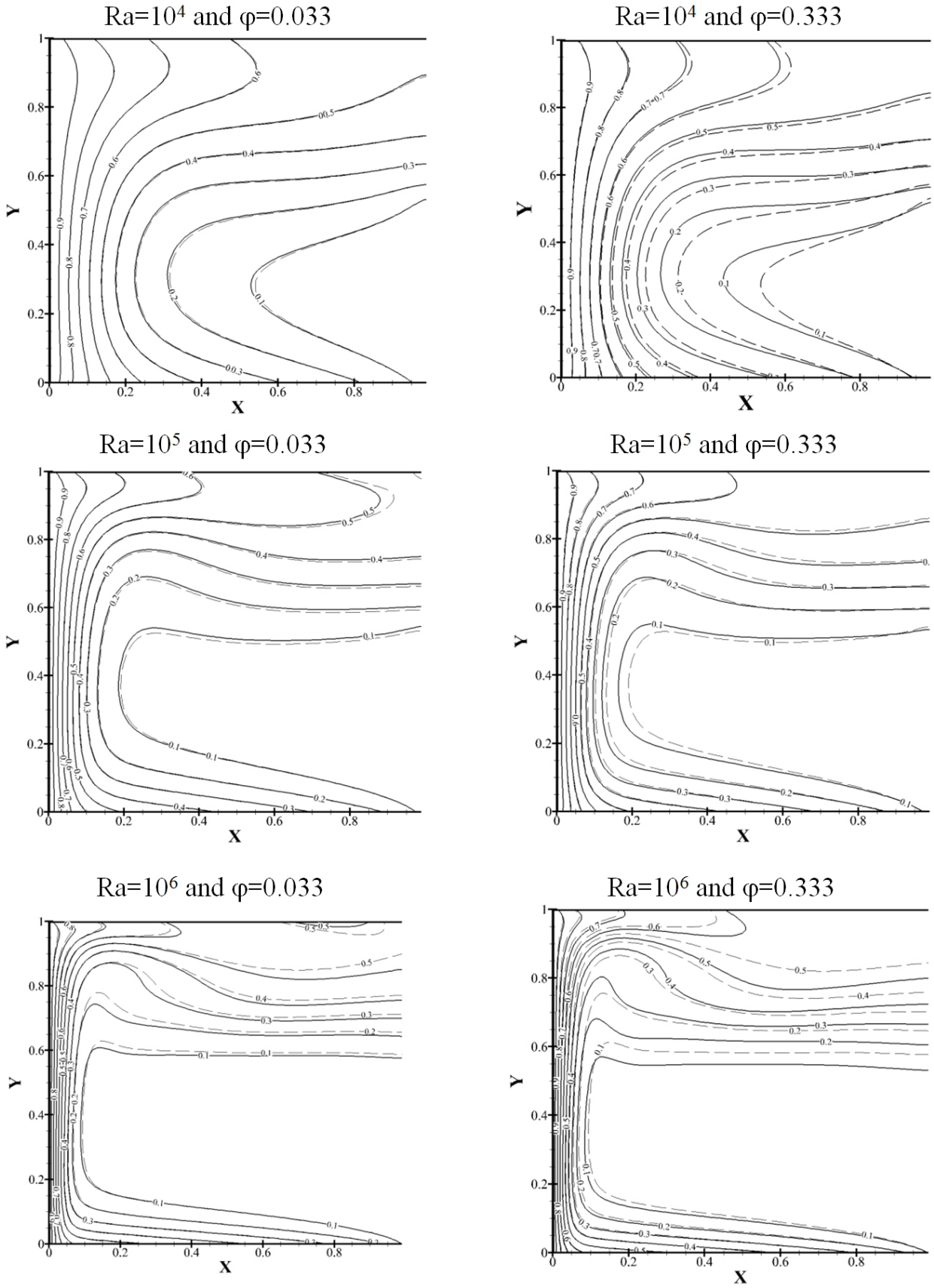

FIGURE 6. Isotherms for the different Rayleigh numbers. The continuous line corresponds to variable properties and the dotted line to the Boussinesq approach.

numbers, but the fluid moves faster for Ra=10^6 as indicated by the density of the streamlines due to the increase in the buoyancy force. However the increasing of the Rayleigh number causes that the upper boundary layer becomes thinner and faster, the velocity of the airflow moving towards the aperture increases, and the area occupied by the leaving hot fluid decreases compared with the one of the entering fluid. Furthermore a very good agreement between the streamlines contours with variable properties and Boussinesq approximation is observed when φ=0.033 for Ra=10^4 and Ra=10^5, but for φ=0.333 the differences between both results is noticeable in the streamlines located in the center of the cavity for all Rayleigh numbers.

The Fig. 4 presents a comparison of the velocity profiles of the Y-component of the velocity at the middle height of the cavity (Y=0.5). When Ra=10^4, the absolute average differences of profiles with variable properties and Boussinesq approach, are between 1.71 % for φ=0.033 and 9.78 % for φ=0.333. However the absolute average differences of profiles for Ra=10^5, are between 4.41 % for φ=0.033 and 14.65% for φ=0.333. Furthermore for Ra=10^6 the absolute average differences between profiles are within 3.42 % for $\varphi = 0.033$ and 30.4% for $\varphi = 0.333$.

The Fig. 5 show the dimensionless isotherms for different values of φ for Ra=10^5, with every graph reporting results with variable properties (continuous line) and with the Boussinesq assumption (dotted line). In all cases, the bottom wall is heated up due to radiation exchange and transfers energy by conduction to the entering fluid. The fluid moves towards the isothermal vertical wall and gains more energy increasing its temperature and moving up. When it reaches the upper adiabatic wall, it changes direction toward the opening of the cavity forming a thermal stratification in the upper part of the cavity, besides the outgoing fluid transfer heat to the wall by conduction and its temperature decreases. On the other hand, by increasing the dimensionless temperature difference, the thickness of the thermal boundary layer on heated wall and the volume occupied by the cold fluid decreases slightly. However for φ=0.033 and φ=0.167, a good agreement between the temperature fields obtained with variable properties and the Boussinesq is observed. The subsequent increment of φ rises the difference between both results.

The effect of the Rayleigh number on the temperature field is displayed in the Fig. 6 for φ=0.033 and φ=0.333. It is noted that by increasing the Rayleigh number, the thickness of the thermal boundary layer next to the hot wall decreases, and the volume occupied by the cold fluid inside the cavity increases. For all considered Rayleigh numbers, when φ=0.033 the temperature fields obtained with variable properties and Boussinesq approximation are very close, while for φ=0.333 noticeable differences are observed.

The dimensionless temperature profiles in the middle height of the cavity (Y=0.5) are shown in Fig. 7. For Ra=10^4, the comparison with the Boussinesq profile indicates absolute average differences between 0.89 % for φ=0.033 and 8.41 % for φ=0.333. However when Ra=10^5 the absolute average differences are between 8.57 % for φ=0.033 and 20.27 % for φ=0.333. The absolute average differences between profiles when Ra=10^6, are within 13.82 % for φ=0.033 and 30.7 % for φ=0.333.

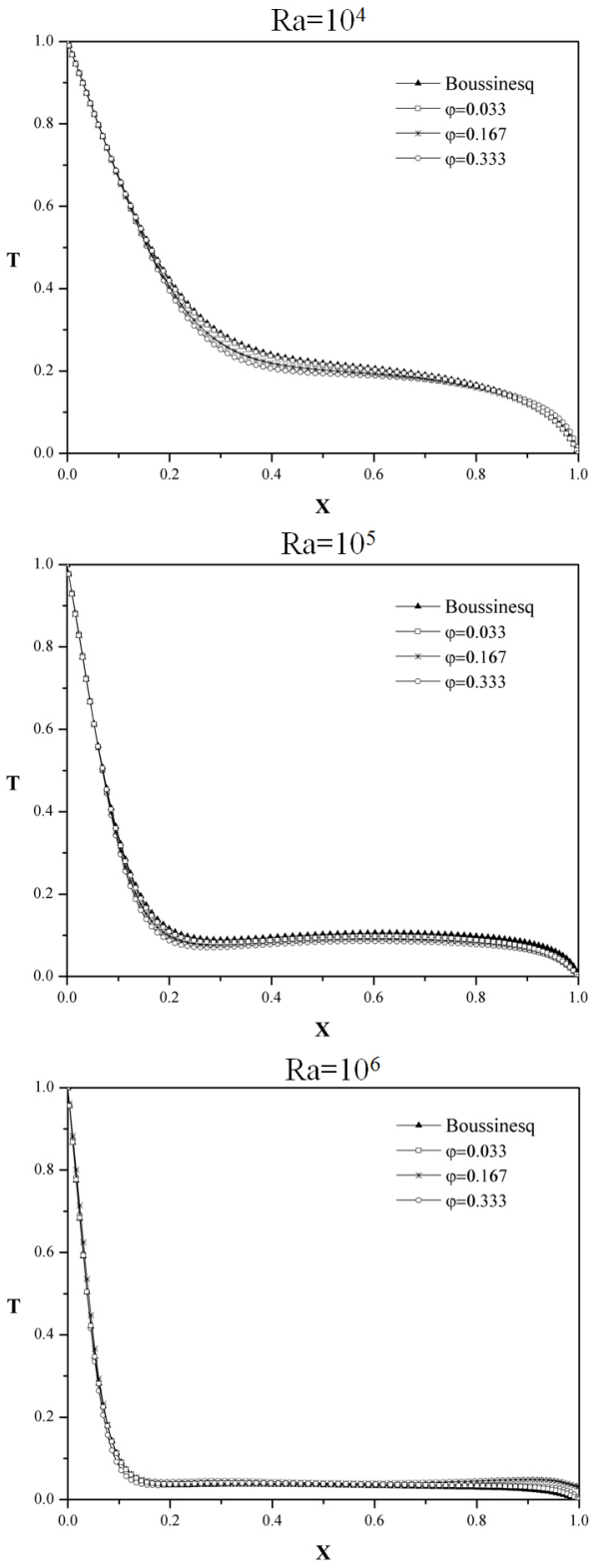

FIGURE 7. Profiles of the dimensionless temperature at Y=0.5.

TABLE IV. Average Nusselt numbers on the hot wall of the open cavity obtained with the Boussinesq approach.

	Ra=10^4			**Ra=10^5**			**Ra=10^6**		
ϕ	$\overline{Nu_c}$	$\overline{Nu_r}$	$\overline{Nu_t}$	$\overline{Nu_c}$	$\overline{Nu_r}$	$\overline{Nu_t}$	$\overline{Nu_c}$	$\overline{Nu_r}$	$\overline{Nu_t}$
0.033	2.98	3.61	6.27	6.39	7.84	13.7	12.54	16.92	28.5
0.167	2.98	2.55	5.53	6.40	5.70	12.1	12.53	12.45	24.9
0.333	2.93	2.78	5.71	6.34	6.22	12.5	12.10	13.25	25.3

TABLE V. Percentage differences between the average Nusselt numbers obtained with variable properties and with the Boussinesq approach.

ϕ	**Ra=10^4**			**Ra=10^5**			**Ra=10^6**		
	Nu$_c$	**Nu**$_r$	**Nu**$_t$	**Nu**$_c$	**Nu**$_r$	**Nu**$_t$	**Nu**$_c$	**Nu**$_r$	**Nu**$_t$
0.033	2.30	1.97	1.88	0.47	2.61	0.22	1.79	3.04	1.49
0.167	4.49	1.16	2.98	1.39	0.00	0.74	0.24	2.30	1.01
0.333	8.15	1.42	4.99	6.90	0.32	3.46	4.42	1.38	1.48

The Table III shows the average Nusselt numbers values considering variable properties. It is showed that with variable properties the average Nusselt numbers increases with both, Rayleigh number and φ. However when the Rayleigh number is varied from 10^4 to 10^6, the average convective Nusselt number increases by 296.9 % for φ=0.333 and 302.5 % for φ=0.167, while the average radiative Nusselt number has increased between 363.5 % for φ=0.333 and 371.7 % for φ=0.167. On the other hand, when φ is varied from 0.033 to 0.333 the differences (considering a fixed Rayleigh number) for the average convective Nusselt number are within 7.08 % for Ra=10^5 to 2.76 % for Ra=10^6, whereas for the average radiative Nusselt are between 15.53 % for Ra=10^5 and 17.38 % for Ra=10^6. Furthermore the total average Nusselt number in the cavity is increased by 328.1 % for φ=0.333 and 333.8 % for φ=0.167 as the Rayleigh number is varied from 10^4 to 10^6. Likewise, the total average Nusselt number in the cavity reduced by 5.04 % for Ra=10^5 and 8.56 % for Ra=10^6 as φ is varied from 0.033 to 0.333.

In order to compare, the average Nusselt numbers values considering the Boussinesq approximation are presented in the Table IV. It can be observed that the Nusselt number remains almost constant or decreases when Rayleigh number and φ are incremented. The previous behavior is explained because the Boussinesq approximation does not take into account the effect of temperature on thermal conductivity near the isothermal wall. However when the Rayleigh number is varied from 10^4 to 10^6, the average convective Nusselt number increases by 313 % for φ=0.333 and 320.8 % for φ=0.033, while the average radiative Nusselt number has increased between 368.7 % for φ=0.033 and 388.2 % for φ=0.167. Whereas when φ is varied from 0.033 to 0.333 the average convective Nusselt number reduces between 0.8 % for Ra=10^5 and 3.5 % for Ra=10^6, furthermore the average radiative Nusselt reduces within 20.7 % for Ra=10^5 and 23.0 % for Ra=10^4. On the other hand the total average Nusselt number in the cavity was found to increase by 344.0 % for φ=0.333 and 355.5 % for φ=0.033 as the Rayleigh number is varied from 10^4 to 10^6. Likewise, the total average Nusselt number in the cavity reduced by 8.5 % for Ra=10^5 and 11.2 % for *Ra*=10^6 as φ was varied from 0.033 to 0.333.

On the other hand, the percentage differences between the Nusselt numbers obtained with variable properties and the values with Boussinesq approach are reported in Table V. The results indicates that for the average convective Nusselt number the differences are between 0.24 % (Ra=10^6 and φ=0.167) and 8.15 % (Ra=10^4 and φ=0.333). Furthermore when comparing the average radiative Nusselt numbers, the differences are between 0 % (Ra=10^5 and φ=0.033) and 2.30 % (Ra=10^6 and φ=0.167). Therefore the variable properties do not affect the radiative exchange in the cavity. Finally the deviations obtained with the Boussinesq approach for the total Nusselt number are within 0.22 % (Ra=10^5 and φ=0.033) and 5 % (Ra=10^4 and φ=0.333).

5. Conclusions

In this paper numerical are compared the numerical calculations of the natural convection and surface thermal radiation, in a square open cavity considering variable fluid properties and Boussinesq approach. From the results we can conclude the following:

The consistency of the flow pattern and temperature field obtained considering variable properties and Boussinesq approximation is good for ϕ=0.033 and ϕ=0.167. However for larger temperature difference the variation is significantly.

When φ=0.033 the average differences between Boussinesq and variable properties for profiles of Y-velocity, are between 1.71 % for Ra=10^4 and 4.41 % for Ra=10^5. However for φ=0.333 the average differences are within 9.78 % for Ra=10^4 and 30.4 % for Ra=10^6.

The comparison of dimensionless temperature profiles with Boussinesq and variable properties, shows that the dif-

ferences are between 0.89 % for Ra=10^4 and 13.82 % for Ra=10^6 when φ=0.033; whereas for φ=0.333 the average differences are within 8.41 % for Ra=10^4 and 30.7 % for Ra=10^6.

For total Nusselt numbers, the results with Boussinesq approach and variable properties, indicates deviations within 0.22 % (Ra=10^5 and φ=0.033) and 5 % (Ra=10^4 and φ=0.333).

Nomenclature

Cp	specific heat capacity, J/kg·K
g	gravitational acceleration, m/s^2
J	radiosity, W/m^2
k	thermal conductivity, W/m-K
L	lenght of the cavity, m
Nu	local Nusselt number
$\overline{Nu}$	average Nusselt number
P	pressure, N/m^2
Pr	Prandtl number
q_r	net radiative heat flux, W/m^2
R	ideal gas constant for air, J/kg·K
Ra	Rayleigh number
T	absolute temeprature, K
T_H	isothermal wall temperature, K
T_∞	ambient temperature, K
U_o	reference velocity, m/s
U,V	dimensionless velocity components
u,v	velocity components, m/s
X,Y	dimensionless coordinates
x,y	coordinates system, m

Greek symbols

α	thermal diffusivity, m^2/s
β	thermal expansion coefficient, 1/K
φ	dimensionless temperature difference
μ	dynamic viscosity, Pa·s
θ	dimensionless temperature
ρ	density, kg/m^3
σ	Stefan-Boltzmann constant, W/m^{2}K

1. P. Le Quere, J.A. Humphrey, and F.S. Sherman, *Numerical Heat Transfer* **4** (1981) 249-283.
2. F. Penot, *Numerical Heat Transfer* **5** (1982) 421-437.
3. J.A. Humphrey, and W.M. To, *Free and mixed convection in a heated cavity, International Journal of Heat and Mass Transfer* **29** (1986) 593-610.
4. D. Angirasa, J.G. Eggels, and F.T. Nieuwstadt, *Numerical Heat Transfer Part A* **28** (1995) 755-768.
5. S.K.S. Boetcher and E. M. Sparrow, *International Journal of Heat and Mass Transfer* **52** (2009) 3850-3856.
6. J. F. Hinojosa, and J. Cervantes de Gortari, *Heat and Mass Transfer* **46** (2010) 595-606.
7. Y.L. Chan, and C.L. Tien, *Numerical Heat Transfer* **8** (1985) 65-80.
8. Y.L. Chan, and C.L. Tien, *International Journal of Heat and Mass Transfer* **28** (1985) 603-612,
9. D. Angirasa, M.J. Pourquié, and F.T. Nieuwstadt, *Numerical Heat Transfer Part A* **22** (1992) 223-239.
10. A.A. Mohamad, *Numerical Heat Transfer Part A* **27** (1995) 705-716.
11. I. Sezai and A.A. Mohamad, *International Journal of Numerical Methods for Heat and Fluid Flow* **8** (1998) 800-813.
12. O. Polat, and E. Bilgen, *International Journal of Thermal Sciences* **41** (2002) 360-368.
13. J.F. Hinojosa, G. Alvarez, C.A. Estrada, *Rev. Mex. Fis.* **52** (2006) 111-119.
14. A.A. Mohamad, M. El-Ganaoui, and R. Bennacer, *International Journal of Thermal Sciences* **48** (2009) 1870-1875.
15. M.A. Hossain, S. Asghar, and R.S.R. Gorla, *International Journal of Numerical Methods for Heat and Fluid Flow* **20** (2010) 759-772.
16. J.O. Juárez, J.F. Hinojosa, J.P. Xamán, and M. Pérez, *International Journal of Thermal Sciences* **50** (2011) 2184-2197.
17. J.L. Lage, J.S. Lim, and A. Bejan, *Journal of Heat Transfer* **114** (1992) 479-486.

18. C. Balaji and S.P. Venkateshan, *International Journal of Heat and Fluid Flow* **15** (1994) 317-324.
19. C. Balaji and S.P. Venkateshan, *International Journal of Heat and Fluid Flow* **16** (1995) 139-144.
20. S.N. Singh and S.P. Venkateshan, *International Journal of Thermal Sciences* **43** (2004) 865-876.
21. J.F. Hinojosa, R.E. Cabanillas, G. Alvarez, and C.A. Estrada, *International Communications for Heat and Mass Transfer* **32** (2005) 1184-1192.
22. J.F. Hinojosa, R.E. Cabanillas, G. Alvarez, and C.A. Estrada, *Numerical Heat Transfer Part A* **48** (2005) 179-196.
23. H. Nouaneguea, A. Muftuoglu, and E. Bilgen, *International Journal of Heat and Mass Transfer* **51** (2008) 6054-6062.
24. J. F. Hinojosa Palafox, *Rev. Mex. Fis.* **58** (2012) 19-28.
25. M. Yang, L. Li and Y. Zhang, *Journal of Heat Transfer* **134** (2012) 09450.
26. O. Polat and E. Bilgen, *International Journal of Heat and Mass Transfer* **46** (2003) 1563-1573.
27. A. Koca, *International Communications in Heat and Mass Transfer* **35** (2008) 1385-1395.
28. M. Miyamoto, T.H. Kuehn, R.J. Goldstein, and Y. Katoh, *Numerical Heat Transfer Part A* **15** (1989) 411-430.
29. A.H. Abib and Y. Jaluria, *International Journal of Heat and Mass Transfer* **38** (1995) 2489-2500.
30. E. Bilgen and H. Oztop, *International Journal of Heat and Mass Transfer* **48** (2005) 1470-1479.
31. K. Vafai and J. Ettefagh, *International Journal of Heat and Mass Transfer* **33** (1990) 2311-2328.
32. K. Vafai and J. Ettefagh, *International Journal of Heat and Mass Transfer* **33** (1990) 2329-2344.
33. K. Khanafer and K. Vafai, *International Journal of Heat and Mass Transfer* **43** (2000) 4087-4100.
34. K. Khanafer and K. Vafai, *International Journal of Heat and Mass Transfer* **45** (2002) 2527-2538.
35. K. Khanafer, K. Vafai, and M. Lighstone, *International Journal of Heat and Mass Transfer* **45** (2002) 5171-5190.
36. A. Andreozzi and O. Manca, *Numerical Heat Transfer Part A: Applications* **57** (2010) 453-472.
37. D.D. Gray and A. Giorgini, *International Journal of Heat and Mass Transfer* **19** (1976) 545-551.
38. Z.Y. Zhong, K.T. Yang, J.R. Lloyd, *Journal of Heat Transfer* **107** (1985) 183-140.
39. M. Modest, *Radiative Heat Transfer*, (McGraw-Hill: New York, USA, 1993).
40. F. P. Incropera and D. P. de Witt, *Fundamentals of Heat and Mass Transfer, Appendix A*, (Wiley and sons, Fourth Edition, 1996).
41. S.V. Patankar, *Numerical Heat Transfer and Fluid Flow*, (Hemisphere Publishing Corporation, 1980).
42. H. K. Versteg and W. Malalasekera, *An Introduction to Computational Fluid Dynamics*. (The Finite Volume Method, Wiley & Sons Inc., 1995).
43. M. Zedan and G. Schneider, *A three-dimensional modified strongly implicit procedure for heat conduction, AIAA* **21** (1983) 295-303.